# Microscopic Vertical Orientation of Nano-Interspaced Graphene Oxide Architectures in Deposit Films as Electrodes for Enhanced Supercapacitor Performance

Gyoung Gug Jang,<sup>1#</sup> Bo Song,<sup>2</sup> Liyi Li,<sup>2</sup> Jong Kahk Keum,<sup>3</sup> Yongdong Jiang,<sup>4</sup> Andrew Hunt,<sup>4</sup> Kyoung-sik Moon,<sup>2</sup> Ching-Ping Wong,<sup>2</sup> Michael Z. Hu<sup>1#\*</sup>

Notice of Copyright This manuscript has been authored by UT-Battelle, LLC under Contract No. DE-AC05-00OR22725 with the U.S. Department of Energy. The United States Government retains and the publisher, by accepting the article for publication, acknowledges that the United States Government retains a non-exclusive, paid-up, irrevocable, world-wide license to publish or reproduce the published form of this manuscript, or allow others to do so, for United States Government purposes. The Department of Energy will provide public access to these results of federally sponsored research in accordance with the DOE Public Access Plan (http://energy.gov/downloads/doe-public-access-plan).

<sup>&</sup>lt;sup>1</sup> Energy and Transportation Science Division, Oak Ridge National Laboratory (ORNL), Oak Ridge, TN 37831

<sup>&</sup>lt;sup>2</sup> School of Material Science and Engineering, Georgia Institute of Technology, Atlanta, GA 30332

<sup>&</sup>lt;sup>3</sup>Center for Nanophase Materials Sciences, Chemical and Engineering Materials Division, ORNL

<sup>&</sup>lt;sup>4</sup>nGimat Co., Norcross, GA 30093

<sup>&</sup>lt;sup>#</sup>Authors of equal contribution.

<sup>\*</sup>Corresponding author: hum1@ornl.gov

#### **Abstract**

This work reported a novel two-step process to fabricate high-performance supercapacitor films that contain microscale domains of nano-interspaced, re-stacked graphene sheets oriented perpendicular to the surface of current collector substrate, i.e., carbon fiber paper. In the two-step process, we first used ligand molecules to modify the surface of graphene oxide (GO) sheets and manipulate the interspacing between the re-stacked GO sheets. The ligand-modified GOs, i.e., m-GOs, were then reduced to obtain more conductive graphene (m-rGO), where X-ray diffraction measurement results indicated well-controlled interlayer spacing between the restacked m-rGO sheets up to 1 nm. The typical lateral dimension of the restacked m-rGO sheets were ~40 µm. Then, electrical field was introduced during m-rGO slurry deposition process to induce the vertical orientation of the m-rGO sheets/stacks in the film deposit. The direct current electrical field induced the orientation of the domains of m-rGO stacks along the direction perpendicular to the surface of deposit film, i.e., direction of electric field. Also, the applied electric field increased the interlayer spacing further, which should enhance the diffusion and accessibility of electrolyte ions. As compared with the traditionally deposited "control" films, the field-processed film deposits that contain oriented structure of graphene sheets/stacks have shown up to ~1.6 times higher values in capacitance (430 F/g at 0.5 A/g) and ~67 % reduction in equivalent series resistance. The approach of using electric field to tailor the microscopic architecture of graphene-based deposit films is effective to fabricate film electrodes for high performance supercapacitors.

**KEYWORDS**: Graphene film deposits, Supercapacitor, Vertically oriented graphene, Functionalized graphene, Graphene interspacing

## Introduction

Graphene-based energy-storage devices such as supercapacitors have attracted rapidly growing attention due to graphene's superior properties (e.g. electrical conductivity, high theoretical surface area and chemical resistance) resulting in high energy density, high rates of charge/discharge, and long cyclic lives. 1 Currently, various engineered graphene electrode platforms have been developed to effectively utilize these intrinsic graphene properties. It can be categorized mainly into two approaches: surface functionalization and structure modification. For surface functionalization, graphene oxide (GO) is mostly used as a precursor for high quality graphene. GO resulting from liquid-phase exfoliation of graphite is suitable for low-cost and mass production of graphene-based particulate materials that contains single or few layer sheets in each particle.<sup>2</sup> However, GO sheets tend to either form irreversible agglomeration or restack during solution reduction process, resulting in significant loss of the surface area. Therefore, various additional ligand molecules, such as surfactant, 3 redox-active functional group molecules, 4,5,6 conductive polymer, 7,8 and transition metallic nanoparticle, 9 have been introduced to prevent the restacking of graphene sheets and increase interlayer spacing (i.e. porous gap) between restacked graphene sheets. Such interspace tailoring for various electrolytes is a strategy to improve the charge storage capability and the wettability of the graphene electrode surface. However, most structures of these graphene electrode materials including reduced GOs (rGOs) are limited to the horizontally aligned film because of intrinsic orientation of two-dimensional graphene sheets. The close restacking of lamellar sheet structure that exists in a dried film retards diffusion of electrolyte ions due to long transport path, resulting in a relatively slow kinetic response.10

For structure modification, three dimensionally architectured graphene films, *e.g.*, porous/holey<sup>11,12,13</sup> and vertically aligned sheets, <sup>10,14,15,16,17,18</sup> have been reported to exhibit high performance supercapacitor electrodes because their enhanced kinetics of electrons and electrolyte ions in their unique structures. Especially vertically-aligned graphene sheets exhibit high kinetic performance due to (1) open edge structure to enhance electron transfer between an active carbon material and a current-collector, (2) a suitable pore size and distribution to facilitate mobility of electrolyte ions, and (3) short paths and ease of electrolyte ions to the graphene layers. Despite these advantages, the fabrication methods for "vertical graphene (VG)" structures such as plasma-enhanced chemical vapor deposition <sup>14,15,16,17,18</sup> and cutting of graphene oxide sheet roll <sup>10</sup> have difficulty in reducing fabrication cost and scale-up for large sized or large amount of films. Furthermore, a low gravimetric capacitance (less than rGO films and powders) because of porosity in free-standing films <sup>10</sup> or densely stacking may limit highly efficient supercapacitors.

In this present work, we report a facile method for depositing VG structured films onto a carbon fiber paper (CFP, as current collector for supercapacitor) by drop-casting and evaporating liquid slurry of molecular ligand composited rGO (m-rGO) under an electrical field (E-field). The graphene surface was first engineered by modifying molecular ligands on GOs and chemically reduced. Four different functional ligand molecules (*e.g.* 2,5-diamino-1,4-dihydroxyl benzene dihydrochloride (DDDC), octadecyltrichlorosilane (ODTS), *p*-phenylenediamine (PPD), polyaniline (PANI)) were studied. The molecular ligands serve as "spacer" to preserve interspace in restacked m-rGO sheets after the film deposits are dried up. The ligand-controlled interspacing increases graphene surface accessibility of electrolytes. The slurry materials of m-rGO dispersed in suitable solvents were drop-casted evaporatively on various substrates (like CFP) under E-

field (Figure 1). The E-field induced vertical orientation of graphene sheets/stacks during the

film deposition/drying. In principle, when a thin 2D graphene sheet is brought into an E-field,

electric polarization effects could induce a moment of force which tends to align the graphene

sheet along the field direction. 19 As described in Figure 1, the appropriate E-field can result in

the formation of a stable vertically-oriented three-dimensional conducting network that avoids

intrinsically tight restacking of graphene sheets due to functionalized ligands. Furthermore, we

observed E-field-tailored interlayer spacing (i.e. widen interspacing relative to baseline m-rGO

films without E-field orientation). These structural and morphological tailoring (at both

nanoscopic and microscopic scales) have led to higher specific capacitance, faster kinetics and

better contact of active material/current collector, compared with a baseline film deposit (i.e.,

horizontally re-stacked graphene film electrode under no E-field).

**Experimental** 

All the chemical reagents in this work were commercially available and used as received. GO

was synthesized from natural graphite powders (230U from Asbury Carbons, PA) by a modified

Hummers method.<sup>20</sup> The 230U is micron sized (~40-50 μm) powder. Carbon fiber paper (CFP,

Spectracarb 2050A - 1050) was purchased from FuelCellsEtc (College Station, TX).

**GO** reduction to r**GO** 

GO and rGO are baseline materials. 100 mg GO was dispersed in 100 ml H<sub>2</sub>O and sonicated for

1 hr, then 1 ml hydrazine (as reducing chemical) was added to the solution and stirred at 80 °C

for 24 hrs. The resulting solution was filtrated and washed with H<sub>2</sub>O repeatedly. The powder was

then dried at 55 °C for overnight.

Synthesis of ligand-grafted graphene: m-rGOs (DDDC-rGO & ODTS-rGO)

5

GO slurry contains 120 mg of GO solid sheets in 40 mL of 200-proof ethanol and was sonicated for 2 hrs to homogenize. 52 μl HCl was added into the slurry and mixed with 150 mg 2,5-diamino-1,4-dihydroxylbenzene dihydrochloride (DDDC) or 200 mg octadecyltrichlorosilane (ODTS) in a reaction vessel sealed with a cap. The reaction mixture was allowed to react at 120 °C in an oven overnight for 16 hrs. The reacted slurry was cooled down to room temperature. For chemical reduction of the ligand-grafted GO, 0.436 ml NH<sub>3</sub> and 35.9 μl hydrazine was dropped into the reaction vessel and the mixture was held at 95 °C for 3 hrs. After cooling at room temperature, the slurry was transferred and centrifuged for 10 min at 12,000 rpm. Supernatant was decanted. The ethanol (~50 mL) washing and centrifugation was repeated 3 times to wash out the residual un-reacted DDDC (purple color) or ODTS.

## Synthesis of m-rGOs (PPD-rGO & PANI-rGO)

PPD-rGO<sup>21</sup> and PANI-GO composite<sup>22</sup> were synthesized by previously reported procedures. For the synthesis of PANI-rGO, reduction was followed by the method of rGO procedure.

## Electric field assisted deposition of particulate films of m-rGO materials

A m-rGO was re-dispersed in ethanol or hexane (only for ODTS-rGO) with sonication for 1 hr to form a homogeneous suspension slurry (~3 g/L). The graphene slurry was drop-casted onto the top surface of a horizontally placed CFP (12 mm of diameter) at the bottom of a "sealed" or "unsealed" glass cell (10 mm of diameter of cylindrical tube), which sits in a vertically oriented E-field at 10 kV (Figure 1 & Figure S1, for the deposition cell configuration). The high voltage was supplied by a high voltage DC power supply (Series ER/DM, Glassman High Voltage, Inc.). The two horizontal parallel electrode plates for generating E-field were ~6 cm diameter of Al foils. The air gap between electrode plates was ~2.5 cm. The slurry of ODTS-rGO or DDDC-rGO was evaporatively deposited onto the CFP top surface in the "sealed" glass cell. (Figure S1)

Once the sealed cell was assembled with a CFP, the drop-casted thin film was formed on the selective area by upward solvent drying under E-field. Other m-rGO material slurries were deposited in the "unsealed" glass cell to reduce deposition rate. (Figure S1). At the beginning of deposition, the porous CFP was drained out some graphene slurry. A continuous graphene film formed on the surface of the CFP via continuous deposition. Once a continuous thin film formed on the porous CFP, the permeate rate of graphene solution was slow down and the film was mainly formed by solvent drying upward under E-field at 10 kV. The drop-casting deposition was repeated to achieve a desirable mass (2~6 mg). A baseline graphene film was deposited as the same way without E-field.

#### **Materials Characterization**

Scanning electron microscopy (SEM) measurement was carried out on a field emission scanning electron microanalyzer (Merlin, Carl Zeiss AG). Fourier transform infrared (FTIR) spectroscopy measurements were carried out on the dry powders using a PIKE diamond crystal ATR on a FTIR spectrometer equipped with a DTGS detector, in the range of 600–4000 cm $^{-1}$ . X-ray diffraction (XRD) measurements were conducted using a PANalytical X'Pert Pro MPD equipped with an X'Celerator solid-state detector. For the XRD measurements, X-rays were generated at 45 kV/40 mA, and X-ray beam wavelength was  $\lambda$ =1.5406 Å (Cu K $\alpha$  radiation).

The interspacing distance (d) of stacked graphene sheets was determined using Bragg equation,  $\lambda=2d\sin\theta$  with  $\lambda$  and  $\theta$  being the X-ray beam wavelength and half of the diffraction angle.

## **Electrochemical Performance Measurement**

Prototype supercapacitors, in the form of coin cells or split cells, were assembled for measuring the electrochemical performance (such as specific capacitance, etc.). For hydrophilic ligand modified graphenes such as DDDC-rGO, PANI-rGO and PPD-rGO, the electrochemical

characterization was conducted under galvanostatic mode in the potential range of 0-0.8Vs with an aqueous electrolyte (1 M H<sub>2</sub>SO<sub>4</sub>), while a hydrophobic ligand modified graphene, ODTS-rGO, and DDDC-rGO were performed in the range of 0-2.5V with an organic electrolyte (1 M tetraethylammonium tetrafluoroborate in acetonitrile). Other control samples including rGO and all other ligand grafted specimens without E-field (at 0 kV) were also tested for comparison. The cell assembly in a symmetrical two-electrode configuration was followed to a previously reported procedure. Electrochemical impedance spectroscopy was performed between 100 kHz and 0.01 Hz. All tests were carried out with a Versastat 2-channel system (Princeton Applied Research).

A specific capacitance is calculated by using the integrated area of the CV curve by:<sup>6</sup>

$$C_{device} = \frac{Q}{\mu \times m \times \Delta V} \times 2$$

Where Q is the integrated area of the CV curve, m is the mass of the active material (g),  $\mu$  is the scanning rate (V/s) and  $\Delta V$  is the potential window of discharge.

The gravimetric capacitance was also calculated from the galvanostatic charge/discharge curves with current density using the formula (for two electrodes thin film configuration): <sup>6,23</sup>

$$C_{device} = \frac{i \times \Delta t}{\Delta V} \times 4$$

Where i(A) is the discharge current,  $\Delta t(s)$  is the discharge time,  $\Delta V(V)$  is the voltage change (exclude the IR drop) within the discharge time, the multiplier of 4 adjust the capacitance of the cell and the combined mass of two electrodes to the capacitance and mass of a single electrode.

## Results and discussion

Under E-field, the deposited film of DDDC-rGO sheets shows vertically oriented graphene sheets/stacks along the E-field direction and the microstructure of the dried film

preserved the orientation architecture. Figure 2a and 2b show the SEM morphological comparison of DDDC-rGO deposits on the CFP with/without E-field (i.e. 10 kV vs 0 kV). 10 kV-oriented graphene sheets form rough and porous surface morphology, resulting from vertically standing graphene sheets (Figure 2a), compared with a relatively smooth surface of a continuous densely stacked film deposited at 0 kV (Figure 2b). The cross-sectional SEM image (Figure 2a') clearly shows vertically oriented microsheet stacks and porous microstructure inside the film and near the top surface of the film (here, "vertical" means in perpendicular to the film surface, i.e., the up-and-down direction in images of Figure 2a'). In the vertically oriented film, some sheets in the film remained in a horizontal direction due to the spatial/rotational hindrance of large sheets. In other words, some m-rGO sheets may not completely rotate/orient along the E-field direction during the evaporative slurry deposition. Thus, we suggest the pores formed by vertically oriented sheets in the film can reduce the diffusion length of electrolyte ions through the graphene film deposit layer to reach the current collector. As expected, the 0 kV-deposited graphene sheets are stacked horizontally after fully dried (Figure 2b'). Besides the DDDC-rGO material, the 10 kV assisted deposition process has created similar vertically re-oriented structure in films of other m-rGO materials such as ODTS-rGO and PANI-rGO (SEM images shown in Supporting Information as Figure S2a & S2b). Depending on functional group and size of composited ligand molecules, the baseline horizontally stacked films (at 0 kV) and the vertically oriented films may show varied structures in porosity and interspacing between stacked sheets. However, it is generally true that the E-field-free deposition always produce horizontally and densely stacked films while 10 kV assisted deposition produce more porous and thicker films that contain vertically oriented m-rGO sheets. Furthermore, we have observed that the E-field seems to facilitate the penetration of graphene sheets into the pores of CFP (Figure S2d). The

penetrated sheets tend to always favorably orient their sheet direction in perpendicular to the surface of CFP.

Figure 3a and 3b show the XRD patterns of DDDC-rGO films deposited on zero background silicon and CFP substrate at E-field=0 and 10 kV, where the patterns of bare GO and CFP substrate were included for references. The XRD patterns of PPD-rGO and ODTS-rGO deposited on CFP substrate were also shown in Figure 3c and 3d. The E-field free DDDC-rGO film deposited on silicon and CFP substrate exhibited broad XRD peaks at  $2\theta=10.37^{\circ}$  (interlayer spacing, d=0.85 nm) and  $2\theta=10.25^{\circ}$  (d=0.86 nm), respectively, which corresponded to (001) reflection of DDDC-rGO. As compared with the peak position of bare rGO,  $2\theta=12.10^{\circ}$  (d=0.73) nm), it is manifested that the added DDDC ligand indeed served as "spacers" on GO surface and increased the interlayer spacing. Another broad XRD peaks at 20=26.49° (0.33 nm) correspond to the moderately aligned graphitic arrays along the [002] direction generated after reduction. The same interspacing control effect was also discerned from the E-field free PPD-rGO, ODTSrGO and PANI-rGO as seen in Figure 3c, 3d and S3, respectively. One of the most interesting features found from the XRD analysis was that the applied E-field widens the interlayer spacing of GO sheets significantly in all the tested films. After E-field-assisted deposition on CFP, the peak positions shifted from 20=10.37° to 10.08° in DDDC-rGO (Figure 3b), from 10.25° to 9.88° in PPD-rGO (Figure 3c) and from 11.58° to 11.08° in ODTS-rGO (Figure 3d), implying that the interlayer spacing increased from d=0.86 nm to 0.89 nm, from 0.93 nm to 0.95 nm and from 0.76 nm to 0.80 nm, respectively. The E-field-assisted widening effect was also observed in the film deposited on Si-substrate as shown in Figure 3a. This is indicated by the shift of diffraction peak from  $2\theta=10.24^{\circ}$  (d=0.86 nm) to  $9.94^{\circ}$  (0.89nm). It is thought that the E-field polarization inhibits a restacking of GO sheets during drying. Here, the facile E-field-assisted

processing method showing the interspacing widening and orientation of GO domains has a very important implication since the method can be used in various binder-free graphene applications to develop high-performance supercapacitors.

FTIR measurements indicated all four ligand molecules were effectively modified on graphene surface (Figure S5). We measured BET surface area of 10 kV-DDDC-rGO and 0 kV-DDDC-rGO electrode films on CFP substrates. The measurable surface area of DDDC-rGOs films were very low ( $< 1 \text{ m}^2/\text{g}$ ) due to organic molecule inhibition to nitrogen adsorption on the surfaces.

In order to assess the E-field derived vertical graphene orientation and interspacing widening effect on electrochemical performance, we have evaluated the film deposits of 10 kVm-rGO (DDDC, PANI, PPD and ODTS) films. Further in-depth characterization of electrical kinetic properties was focused on DDDC-rGO. Figure 4a shows the CV curves of DDDC-rGO electrodes measured at the same scan rate at 10 mV/s for 10 kV-oriented specimen (active material mass; 2.6 mg/cm<sup>2</sup>) and non-oriented one (2.7 mg/cm<sup>2</sup>). At the similar mass loading, the gravimetric capacitance value of the electrode film deposited at 10 kV (the integrated curve area) is larger than 0 kV-electrode. It indicates the specific capacitance of the 10 kV-electrode is 260 F/g which is ~1.6 times higher than 168 F/g of 0 kV-electrode. Figure 4b shows the galvanostatic charge/discharge plots for 0 kV and 10 kV electrodes with the same loading amount at 1 A/g. The charge and discharge curve of 10 kV-electrode exhibits ~1.5 time longer than 0 kV. It results in 391 F/g, which is higher than 304 F/g of 0 kV-electrode. Also, the specific capacitance enhancement effect via E-field orientation was evaluated with varying deposit loading amount of active materials (Figure 4c). It was reported that specific capacitance of rGO films decrease with thickness. 10 The similar trend of loading effect is also observed in 0 kV and 10 kV-DDDC-rGO

electrodes. The specific capacitances of both DDDC-rGO electrodes decrease with increase of loading amount. Interestingly, 10 kV-orientation enhances its capacitance at each loading amount. The smallest loading amount (1.2 mg/cm²) has the highest capacitance value of 393 F/g at 5 mV/s (430 F/g at 0.5 A/g), which is ~1.3 times higher than a referential 0 kV-DDDC-rGO. The highest loading of 10 kV (4.1 mg/cm²) decreased to 185 F/g at 5 mV/s. However, the value is still ~1.2 times higher than non-oriented DDDC-rGO at the similar loading.

The enhanced capacitance of 10 kV-DDDC-rGO electrodes could be explained by exposed edge of oriented graphene sheets and widened interlayer spacing. Such exposed graphene edge effect was previously reported to produce higher specific capacitance, faster electron transfer rate and stronger electro-catalytic activity relative to basal plane surfaces. 10,14,15,24,25 Also, the enlarged interlayer spacing could be another contribution of this improvement via increase of the charge-storage capability between stacked sheets. This result agrees with literature finding that the larger sized surfactant ligand intercalated rGO showed higher specific capacitance.<sup>3</sup> For 10 kV-PPD-rGO, the vertical re-orientation of sheets is hard to be visualized by SEM imaging (Figure S2c), however XRD peak shifting to low angle (meaning enlargement of intercalation gap) is observed (Figure 3c). In spite of no obvious visual structural re-arrangement, the specific capacitance of 10 kV-PPD-rGO shows significant (~20%) improvement compared to 0 kV (Table 1). Thus, it is reasonable to interpret that the E-field oriented interspacing enlargement could be a factor for the improvement of the capacitance via more charge-storage effect between restacked graphene sheets. Different voltages assisted electrodes below 10 kV (such as 5kV) were developed, however we did not observe significant enhancement effect on capacitance in this system.

Besides the impact on capacitance values, the vertically oriented 10 kV-DDDC-rGO electrode exhibited higher electron/ion transport performance, compared to non-oriented electrodes. Figure 4b showed that the voltage (IR) drop of the film deposited at 10 kV was 0.11 V which is lower than 0.14 V of the film deposited at 0 kV. The similar features of reduced IR drop were also observed at low and high loading electrodes (~1.2 & ~4.2 mg/cm<sup>2</sup>: Table S1). For 10 kV vs. 0 kV, they show 0.05 vs. 0.06 and 0.13 vs. 0.21 at  $\sim$ 1.2 and  $\sim$ 4.2 mg/cm<sup>2</sup>, respectively. Generally, the both IR drops increase with loading amount. The reduced IR drop indicates that the capacitive reversibility is high, attributed by the high-quality contact at the interface of active material/current collector. 10,15 Furthermore, comparing with asymmetric charging/discharge curve of 0 kV-DDDC-rGO, the charging/discharging curves of 10 kV are more symmetric, indicating the capacitive reversibility was high, consistent with its electrochemical characteristics. Nyquist plot, as shown in Figure 4d, indicates the kinetic features of electron transfer/ion diffusion at the electrodes. The slopes of 10 kV-DDDC-rGOs in comparison with the curves of 0 kV was higher in the low frequency region, suggesting higher ion diffusion behavior, Warburg impedance, due to the vertically oriented and open-edge structured electrode. <sup>10,15,17</sup> The first and second intersects of semicircle curve in the high frequency region of the Nyquist plot implies the equivalent series resistance (ESR;  $R_s$ ) and charge transfer resistance ( $R_{ct}$ ), respectively. For the ion response, the film deposited at 10 kV showed  $\sim 50$  % low resistance ( $R_s$ = 2.6  $\Omega$ ) in comparison with the film deposited at 0 kV ( $R_s$  = 5.6  $\Omega$ ) at the same medium loading amount. The low  $R_s$  implies an improved electrical conductivity at the interface between electrode and electrolyte. The similar features of higher ion diffusion and lower resistance were also observed at low and high loading electrodes (~1.2 & ~4.2 mg/cm<sup>2</sup>: Table S1 & Inset of Figure 4d). Note that the high loading of active material in electrode (~4.2 mg/cm<sup>2</sup>) achieved the

smallest  $R_s$  (0.49  $\Omega$ ) which ~67% less than the  $R_s$  for baseline sample at 0 kV (1.5  $\Omega$ ). It suggests that the loading amount is a critical factor to determine the kinetics in electrodes. Generally, the material and texture of current collector affect the interface resistance between active material and current collector.  $^{11,15}$  We expect the  $R_s$  of E-field oriented deposit will be effectively reduced on metallic foil current collectors. The dependence of the phase angle on frequency (Bode phase plot) for 10 kV- and 0 kV-DDDC-rGO is shown in Figure 4e. At the same loading, the characteristic frequency,  $f_0$ , of 10 kV for phase angle of 45° (the equal point for the resistive and capacitive impedances) is 0.022 Hz (corresponding elapsed time; 45.7s) which is higher than 0.017 Hz of 0 kV (58.0s). The rapid frequency response suggests that the vertically oriented structure of 10 kV-DDDC-rGO enhance the electrolyte ion transport rate. For the response time, the electrode sample with the low loading amount of 1.2 mg/cm<sup>2</sup> appears to be more effectively affected by E-orientation. The elapsed time of the film deposited at 10 kV was 5.5 s which is faster than 21.2 s of the film deposited at 0 kV (Inset of Figure 4e). At the high loading of ~4.2 mg/cm<sup>3</sup>, the elapsed time of the film deposited at 10 kV was 56 s which is faster than >100 s of the film deposited at 0 kV. Figure 4f shows the capacitance retention (with respect to 5 mV/s) with increasing scan rates. At higher scanning rate, the ion mobility generally decreases in carbon-based capacitor electrodes, resulting in decrease of capacitance. 4,10 It appears E-field orientation cannot effectively improve the capacitance retention at high scan rate. Both the electrode films deposited at 10 kV and 0 kV show a similar decrease pattern. Instead, the lower loading amount improves the capacitance retention. Due to structural hindrance with large size of intrinsic graphene sheets, the 10 kV E-field did not orient sheets vertically on entire electrode. Control of graphene size with E-field strength expects to increase vertical orientation ratio on the

electrode. It may improve the ion mobility in the further oriented electrode structure and improve the capacitance retention.

To investigate the cycling stability of the 10 kV-oriented and 0 kV-non-oriented DDDC-rGO electrodes, galvanostatic charge-discharge cycling was performed for 8000 cycles at a current density of 2 A/g (Figure 5). The results reveal that both the electrodes deposited at 10 kV and 0 kV show high long term cycling stability. Specifically, the capacitance decay of the electrodes deposited at 10 kV and 0 kV was 92 % and 89 % of the initial discharge capacitance retained after 8000 cycles, respectively. It indicates that the polymer binder-free vertically oriented electrode structure exhibits the long-term electrochemical stability.

Table 1 shows the summarized average specific capacitance of all other m-rGOs electrodes with aqueous and organic electrolytes. Including DDDC-rGO, other m-rGOs (i.e. PPD, and ODTS) exhibits the enhanced capacitance via E-field orientation. Compared to aqueous electrolyte, the larger molecule size of organic electrolytes shows 26~29% of the capacitances retained from aqueous electrolyte. However, it appears that the organic electrolyte coin cell of 10 kV-electrode still exhibits E-field orientation effect resulting in higher capacitance compared with 0 kV-DDDC-rGO. The 10 kV-PPD and ODTS-rGO, as it mentioned earlier, show the E-field orientation effects, resulting in higher specific capacitance than non-oriented electrodes. 10kV-PANI-rGO shows similar capacitance values of 0 kV-electrode. However, galvanostatic charge/discharge curves of 10 kV-PANI-rGO exhibit symmetric charging/discharging characteristics (*i.e.* ideal capacitance feature) while 0 kV-electrode exhibits asymmetric feature with gradual charge curve (Figure S6b). In addition, IR drop of 10 kV (0.164 at 1 A/g) is much lower than 0 kV (0.287 at 1 A/g). Including the vertical orientation and interspacing control via E-field, the 10 kV-PANI-rGO exhibits additional new crystal

morphology, a crystal peak augmentation (Figure S3). These crystalline features may contribute to the unique charge-discharge performance. It suggests that depending on binding molecules, the associated E-field orientation revealed different performance effects. The optimization of ligand composition ratio could increase the capacitance, but it was out of scope in our study. Note that rGO powder deposits did not show E-field alignment effect due to agglomeration of graphene particles after drying. Additional capacitance comparison of E-field oriented DDDC-rGO electrodes results is available in Table S1. 10% of polymer (*i.e.* PVDF) was added in DDDC-rGO solution. The polymer bounded DDDC-rGO also exhibits capacitance improvement, compared to non-oriented one. The summarized capacitance feature indicates the E-field orientation is a facile and versatile approach developing morphology changes applicable to other ligands modifying GO.

## **Conclusion**

This work demonstrated that molecular ligand modified graphene sheets/stacks could serve as a molecular engineering approach to accommodating the nanoscale interspacing of restacked graphene in the film deposit. On the other hand, external field-induced vertical orientation of graphene sheets represents a new engineering approach to tailoring the microscopic architecture of the films, resulting in improved supercapacitor electrode performance. The graphene film electrodes based on vertical orientation structure and interlayer spacing controlled by various ligands are easily prepared using a facile E-field orientation-deposition process. Various E-field oriented graphene electrodes have shown the improvement of electrochemical characteristics, higher capacitance and transport performance, in comparison with non-oriented film electrodes. More optimization based on deposition conditions and active materials (such as ligand type,

grafting amount, solvent type, concentration in slurry, graphene sheet size to reduce space hindrance) will be the subject for future investigation.

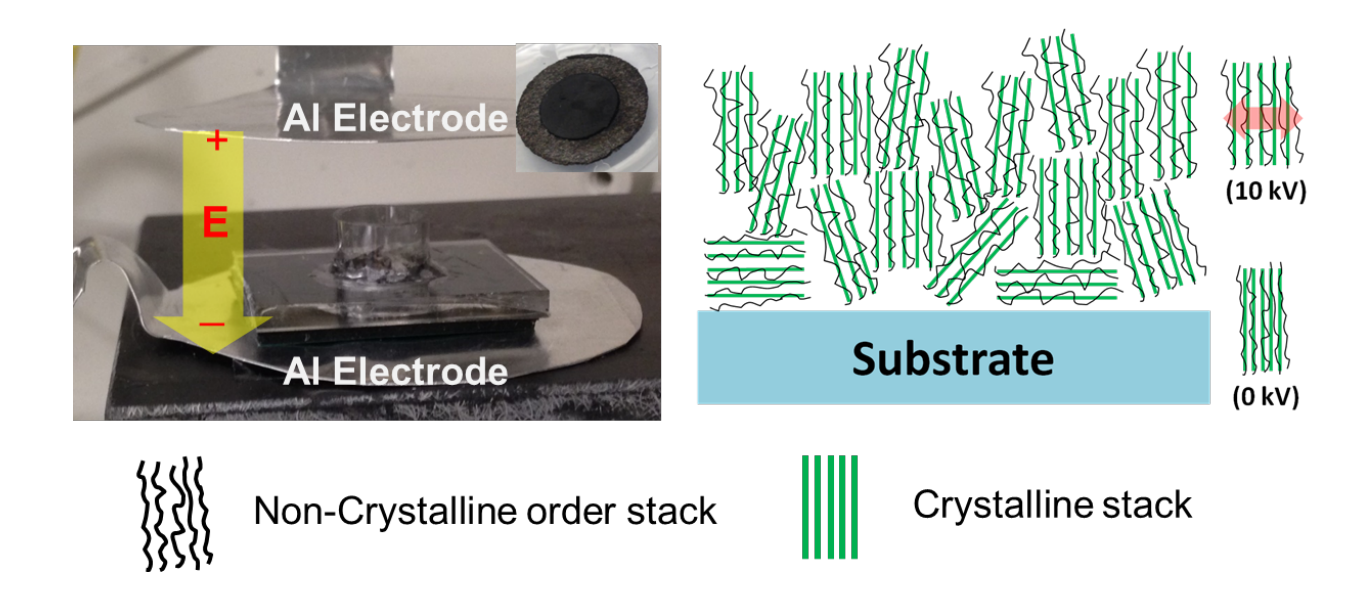


**Figure 1** Two-step process to deposit graphene films that contain controlled nano-interspacing and microscopic "vertical graphene" domains (i.e., non-crystalline order stack or crystalline stack). Vertical structures evolve during electrical field-assisted deposition of m-rGO films under electric field at 10 kV.

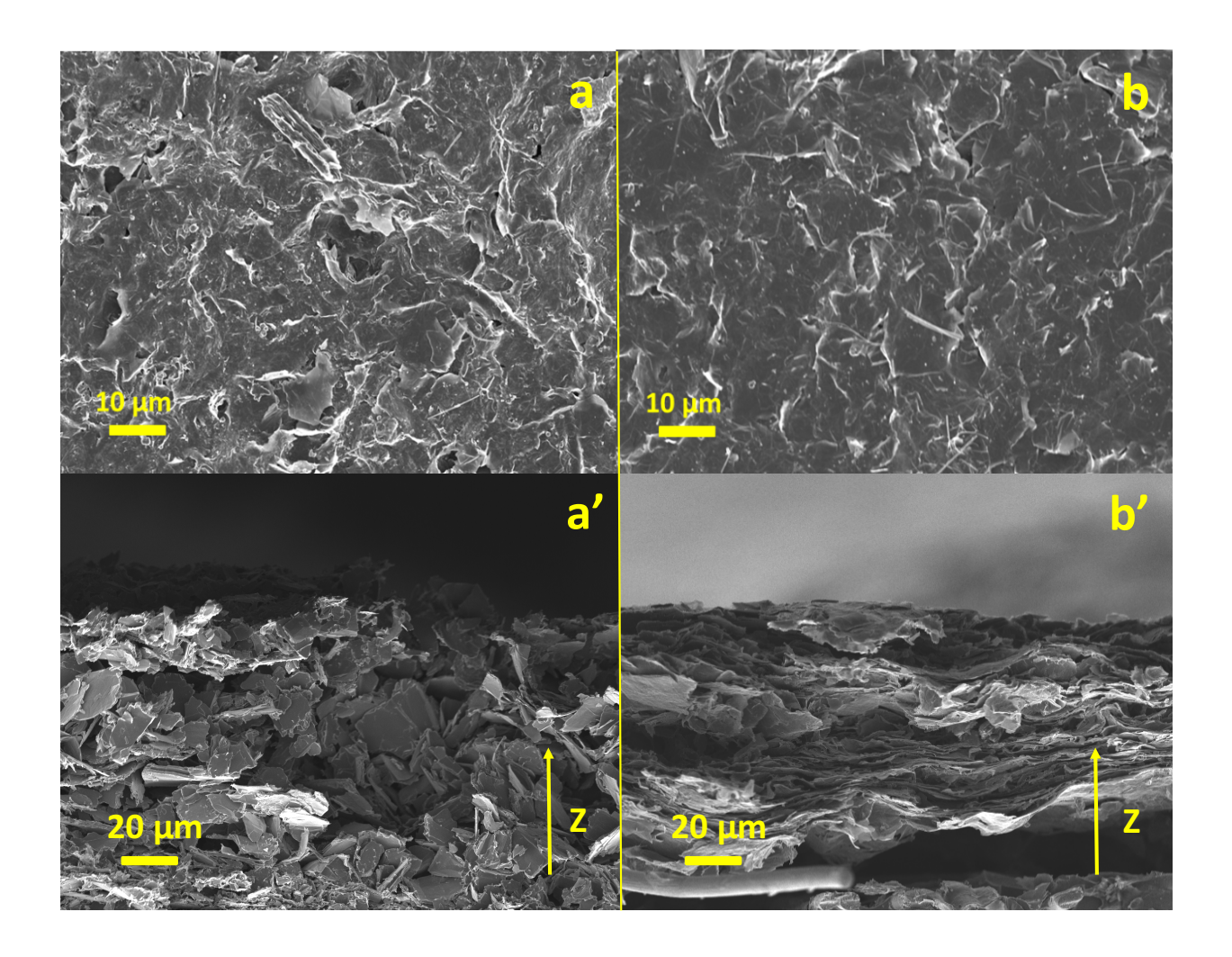


**Figure 2** Micro-morphology of deposited films of DDDC-rGOs with/without electric field (0kV vs 10 kV). (a) Top surface view and (a') Cross-section view of DDDC-rGO film deposited at 10 kV; (b) Top surface view and (b') Cross section view of a baseline "control" DDDC-rGOs film at 0 kV. Image a' clearly shows the vertical orientation of some graphene sheets/stacks along the z direction (i.e., electrical field line direction). Image b' shows the horizontal stack of graphene sheets in a traditional film deposit sample.

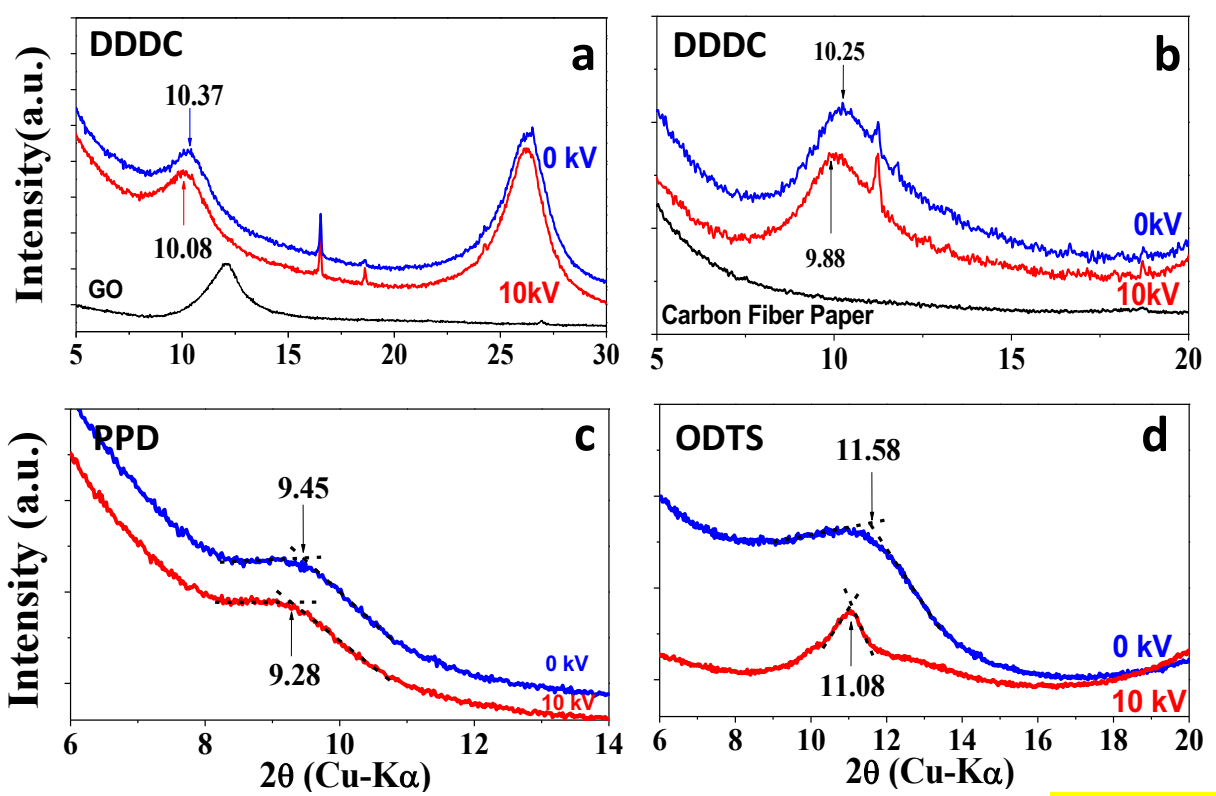


**Figure 3** X-Ray diffraction patterns of electric field assisted m-rGO films and films deposited at 0 kV (a) DDDC-rGO deposited on a zero-background silicon substrate, (b) DDDC-rGO deposited on carbon fiber paper, (c) PPD-rGO on carbon fiber paper and (d) ODTS-rGO on carbon fiber paper.

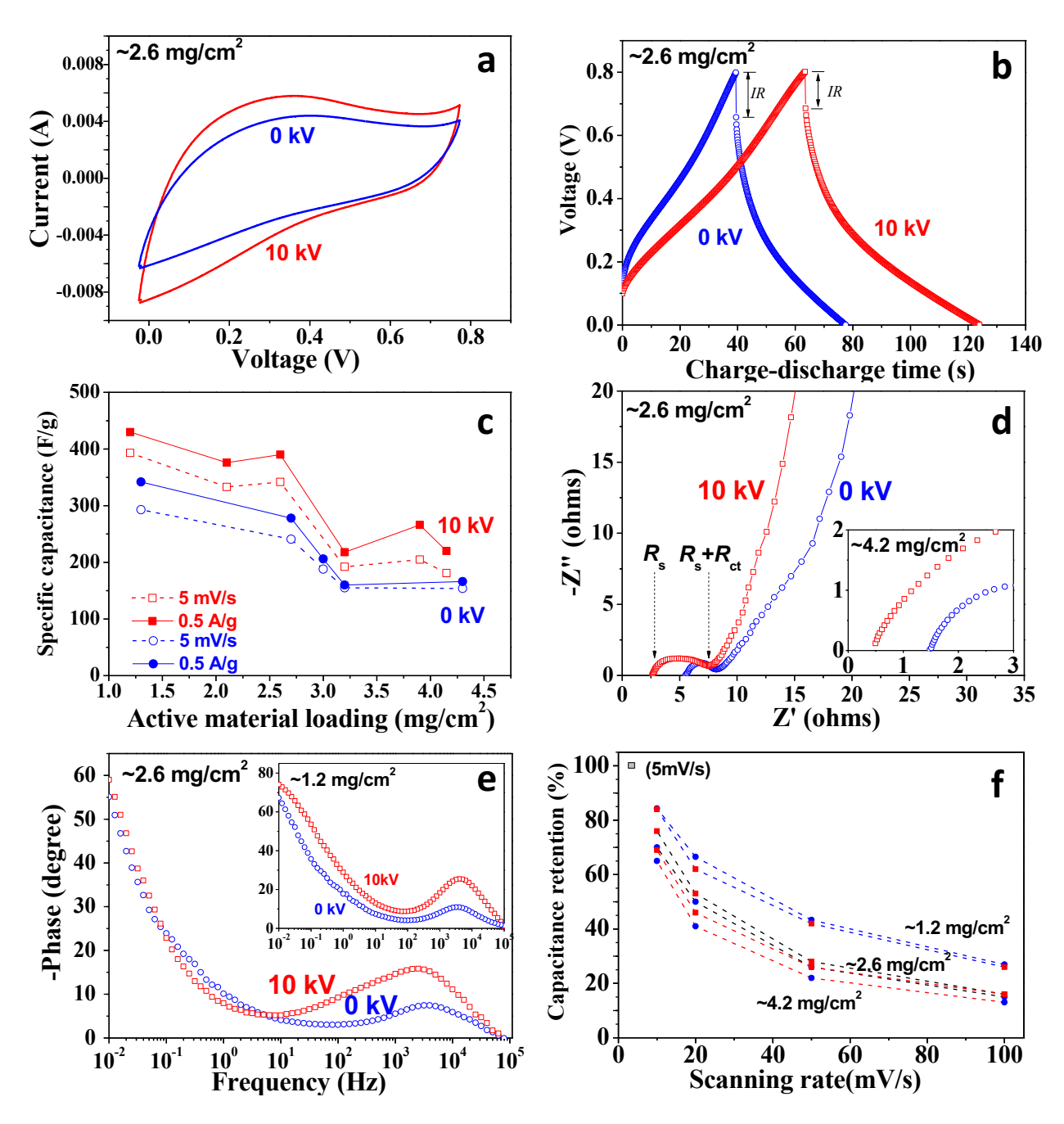


**Figure 4** Supercapacitor performance of 10 kV-field oriented versus 0 kV- non-oriented DDDC-rGO film in a two electrode system with 1.0 M H<sub>2</sub>SO<sub>4</sub> electrolyte. (a) CV curves at a scan rate of 10 mVs<sup>-1</sup>; (b) Galvanostatic charge/discharge curves at a current density of 1.0 A/g; (c) Specific capacitance comparison as function of deposit loading amount; (d) Nyquist plot, Inset is a high frequency region of high loaded electrodes (~4.2 mg/cm<sup>2</sup>) (e) Bode plots of phase angle versus frequency, Inset is low loaded electrodes (~1.2 mg/cm<sup>2</sup>) (f) Relative specific capacitance retention as function of scan rates and loading amounts

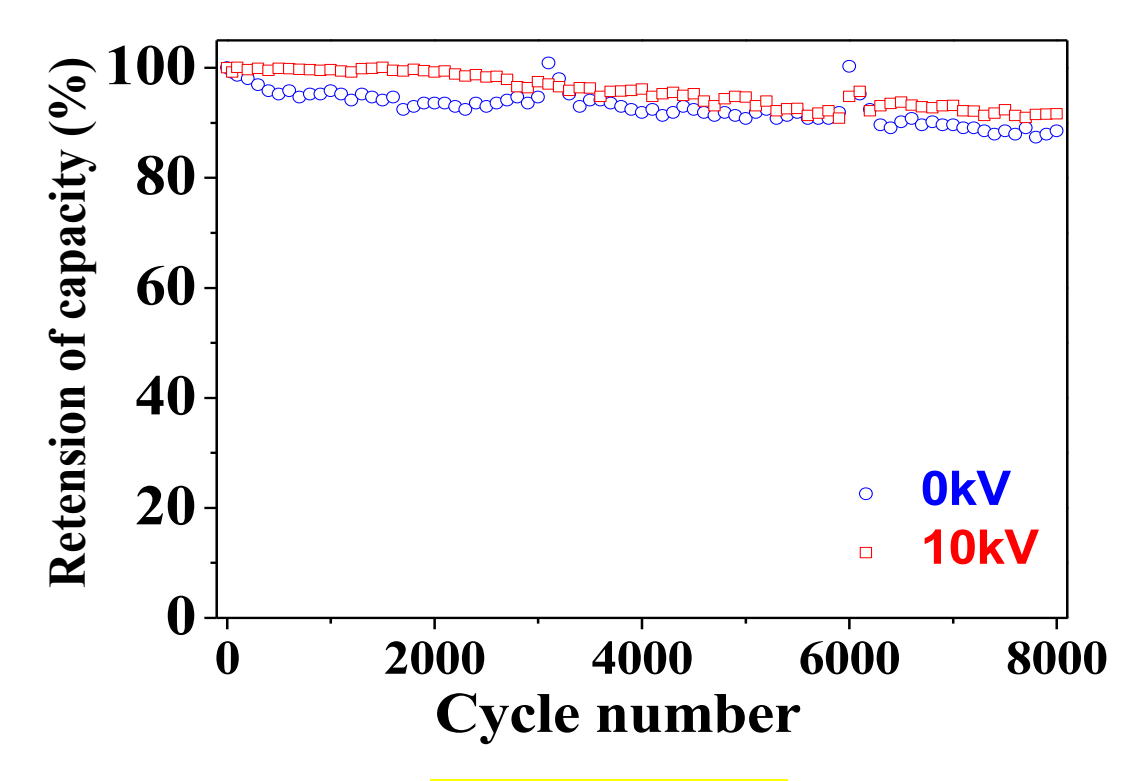


Figure 5 Cycling performance of DDDC-rGO film electrodes measured at 2.0 A/g

Table 1 Comparison of molecular ligand-modified rGO capacitance at 0 kV and 10 kV.

Name		5mV/s	10 mV/s	20  mV/s	50 mV/s	100 mV/s	Loading (mg/cm²)
DDDC1	0kV	241	168	121	63	35	2.7
	10kV	341	260	179	95	54	2.6
DDDC <sup>2</sup>	0kV	-	26	18	10	6	2.7
	10kV	-	72	49	25	14	2.6
PPD <sup>1</sup>	0kV	-	214±24	145±16	80±7	51±4	2.6 ±0.2 (n=4)
	10kV	-	254±25	177±16	92±8	52±4	2.3±0.4 (n=5)
PANI <sup>1</sup>	0kV	262	239	195	99	50	4.2
	10kV	251	242	198	112	52	3.9
ODTS <sup>2</sup>	0kV	-	31	-	11	6	9.6
	10kV	-	40	-	20	12	9.2
BarerGO	0kV	-	62	46	26	-	9.7
	10kV	-	60	39	17	-	10.0

<sup>1)</sup> Split cell; 1M H<sub>2</sub>SO<sub>4</sub>, 2) Coin cell; 1M Tetraethylammonium tetrafluoroborate in acetonitrile

**Conflict of interest**: The authors declare no completing financial interest

Acknowledgement: This research work was supported by the Advanced Research Project

Agency-Energy (ARPA-E) Program # DE-AR0000303. Part of the materials characterization

(including XRD and SEM) was conducted at the Center for Nanophase Materials Sciences,

which is sponsored by the ORNL Scientific User Facilities Division and DOE Office of Basic

Research Sciences. The development of graphene coating deposition method was also partially
sponsored by the DOE/BETO program due to interest in graphene coated membrane
development and applications.

**Supporting Information Available**: 1) Summary of E-field aligned DDDC-rGOs capacitance 2) Deposit Cell configuration 3) Characterization of SEM, XRD and FTIR4) Further electrochemical characteristics for electrode materials. This material is available free of charge via the internet at http://pubs.asc.org

## Reference

- [1] K.S. Novoselov, V.I. Fal'ko, P.R. Gellert, M.G. Schwab, K. Kim, Nature 490 (2012) 192.
- [2] B. Xu, S. Yue, Z. Sui, X. Zhang, S. Hou, G. Cao, Y. Yang, Energy Environ. Sci. 4 (2011) 2826.
- [3] K. Zhang, L. Mao, L.L. Zhang, H.S.O. Chan, X.S. Zhao, J. Wu, J. Mater. Chem. 21 (2011) 7302.
- [4] W. Ai, W. Zhou, Z. Du, Y. Du, H. Zhang, X. Jia, L. Xie, M. Yi, T. Yu, W. Huang, J. Mater.
  Chem. 22 (2012) 23439.
- [5] J.H. Lee, N. Park, B.G. Kim, D.S. Jung, K. Im, J. Hur, J.W. Choi, ACS Nano 7 (2013) 9366.
- [6] L. Li, B. Song, L. Maurer, Z. Lin, G. Lian, C.C. Tuan, K.S. Moon, C.P. Wong, Nano Energy 21 (2016) 276.
- [7] J. Yan, L. Yang, M. Cui, X. Wang, K.J. Chee, V.C. Nguyen, V. Kumar, A. Sumboja, M. Wang, P.S. Lee, Adv. Energy Mater. 4 (2014) 1400781.
- [8] B. Song, L. Li, Z. Lin, Z.K. Wu, K.S. Moon, C.P. Wong, Nano Energy 16 (2015) 470.
- [9] S.S. Kim, Y.R. Kim, T.D. Chung, B.H. Sohn, Adv. Funct. Mater. 24 (2014) 2764.
- [10] Y. Yoon, K. Lee, S. Kwon, S. Seo, H. Yoo, S. Kim, Y. Shin, Y. Park, D. Kim, J. Choi, H. Lee, ACS Nano 8 (2014) 4580.
- [11] L.L. Zhang, X. Zhao, M.D. Stoller, Y. Zhu, H. Ji, S. Murali, Y. Wu, S. Perales, B. Clevenger, R.S. Ruoff, Nano Lett. 12 (2012) 1806.
- [12] Y. Lin, X. Han, C.J. Campbell, J.W. Kim, B. Zhao, W. Luo, J. Dai, L. Hu, J.W. Connell, Adv. Funct. Mater. 25 (2015) 2920.
- [13] Z. Li, B. Song, Z. Wu, Z. Lin, Y. Yao, K.S. Moon, C.P. Wong, Nano Energy 11 (2015) 711.

- [14] J.R. Miller, R.A. Outlaw, B.C Holloway, Science 329 (2010) 1637.
- [15] Z. Bo, W. Zhu, W. Ma, Z. Wen, X. Shuai, J. Chen, J. Yan, Z. Wang, K. Cen, X. Feng, Adv. Mater. 25 (2013) 5799.
- [16] Z. Bo, S. Mao, Z.J. Han, K. Cen, J. Chen, K. Ostrikov, Chem. Soc. Rev. 44 (2015) 2108.
- [17] M. Cai, R.A. Outlaw, R.A. Quinlan, D. Premathilake, S.M. Butler, J.R. Miller, ACS Nano 8 (2014) 5873.
- [18] Q. Liao, N. Li, S. Jin, G. Yang, C. Wang, ACS Nano 9 (2015) 5310.
- [19] Z. Wang, Carbon 47 (2009) 3050.
- [20] D.C. Marcano, D.V. Kosynkin, J.M. Berlin, A. Sinitskii, Z. Sun, A. Slesarev, L.B. Alemany, W. Lu, J.M. Tour, ACS nano, 4 (2010) 4806.
- [21] X. Lu, L. Li, B. Song, K.S. Moon, N. Hu, G. Liao, T. Shi, C.P. Wong, Nano Energy 17 (2015) 160.
- [22] Z. Lin, G. H. Waller, Y. Liu, M. Liu, C.P Wong, Carbon 53 (2013) 130.
- [23] N.D. Kim, D. Buchholz, G. Casillas, M. Jose-Yacaman, R.P.H. Chang, Adv. Func. Mater. 24 (2014) 4186.
- [24] W. Yuan, Y. Zhou, Y. Li, C. Li, H. Peng, J. Zhang, Z. Liu, L. Dai, G. Shi, Sci. Rep. 3 (2013) 2248.
- [25] W. Song, X. Ji, W. Deng, Q. Chen, C. Shen, C.E. Banks, Phys. Chem. Chem. Phys. 15 (2013), 15, 4799.